

Map-Free Visual Relocalization Enhanced by Instance Knowledge and Depth Knowledge

Mingyu Xiao¹ Runze Chen¹ Haiyong Luo² Fang Zhao¹
Juan Wang³ Xuepeng Ma³

¹ Beijing University of Posts and Telecommunications

² Institute of Computing Technology, Chinese Academy of Science

³ Shouguang Cheng Zhi Feng Xing Technology

{ShawnMY, chenrz925, zfsse}@bupt.edu.cn yhluo@ict.ac.cn

{wang.juan.2024, ma.xuepeng.2024}@outlook.com

Abstract. Map-free relocalization technology is crucial for applications in autonomous navigation and augmented reality, but relying on pre-built maps is often impractical. It faces significant challenges due to limitations in matching methods and the inherent lack of scale in monocular images. These issues lead to substantial rotational and metric errors and even localization failures in real-world scenarios. Large matching errors significantly impact the overall relocalization process, affecting both rotational and translational accuracy. Due to the inherent limitations of the camera itself, recovering the metric scale from a single image is crucial, as this significantly impacts the translation error. To address these challenges, we propose a map-free relocalization method enhanced by instance knowledge and depth knowledge. By leveraging instance-based matching information to improve global matching results, our method significantly reduces the possibility of mismatching across different objects. The robustness of instance knowledge across the scene helps the feature point matching model focus on relevant regions and enhance matching accuracy. Additionally, we use estimated metric depth from a single image to reduce metric errors and improve scale recovery accuracy. By integrating methods dedicated to mitigating large translational and rotational errors, our approach demonstrates superior performance in map-free relocalization techniques.

1 Introduction

Visual relocalization is a technology that emulates the human ability to estimate the position and orientation of a camera from a single query image. This task has been extensively researched and offers numerous exciting applications in augmented reality (AR) and robotic navigation. By leveraging this technology, we can achieve more precise location awareness and navigation in complex environments, significantly enhancing both the technological capabilities and user experience in these domains. Traditional map-based visual relocalization techniques [31] require a large number of images and scale calibration to create detailed 3D maps of scenes. However, the necessity of creating detailed 3D

maps limits their application, particularly in scenarios requiring extensive memory resources. Unlike traditional relocalization methods, map-free relocalization aims to determine the camera pose of a query image given a reference image, eliminating the need for pre-built maps. Map-free methods require fewer images and eliminate the need to construct a 3D map. However, this lack of multi-view constraints imposes limitations, as it relies solely on features extracted from two images for computation and relocalization, presenting a significant challenge. A common attempt is to utilize various techniques to achieve better matching performance [30, 33, 41]. However, the underlying mechanism for achieving better performance of map-free relocalization needs more exploration.

To gain a deeper understanding of the performance of existing map-free models, we conducted a detailed analysis of existing methods mentioned in Map-free Visual Relocalization [2]. These methods consist of three components, feature matching, pose estimation modules, and depth estimation. We show some of the results in Figure 1. Based on these experimental results, we draw the following conclusions: Firstly, as indicated by the blue points in Figure 1, different feature point matching methods result in variations in both translation and rotation errors, underscoring the importance of accurate feature point matching. This is because the essential matrix is calculated from the coordinates of matched feature points. The rotation matrix and translation vector, which determines the performance of visual relocalization, are derived directly from this essential matrix. Secondly, As illustrated by the red dots in Figure 1, variations in the depth estimation method result in significant changes in translation error, while rotation error remains almost unchanged. This occurs because the depth estimation module projects 2D feature points into 3D space using the depth estimation results. By estimating the distances between feature points in 3D space, the scale of the translation vector obtained in the previous step can be accurately recovered. This comprehensive study of the interplay between feature matching and depth estimation within map-free models provides insights into enhancing overall performance.

To improve the accuracy of map-free relocalization, we propose a novel framework that not only enhances matching precision but also effectively addresses the challenges of metric depth estimation. This comprehensive approach signif-

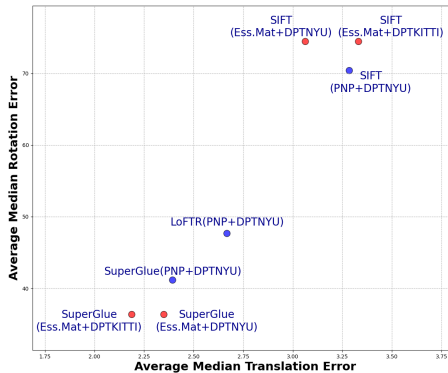


Fig. 1: Average median translation and average median rotation errors compared between the method employing only replacement feature point matching (depicted as blue dots) and the method utilizing solely replacement depth estimation (depicted as red dots).

icantly advances visual relocalization by systematically reducing both rotation and translation errors, which are critical for achieving reliable localization without the need for pre-existing maps. For rotation errors, our method leverages the extraction of matching points within instance objects. By guiding the feature point matching model to focus on specific instance matches, we can effectively minimize incorrect matches that typically occur among different instances. This targeted approach not only reduces the error rate but also boosts the overall accuracy and reliability of the matching process. For translation errors, our framework incorporates an advanced depth estimation technique. This technique employs standard camera transformations and joint depth-normal optimization to tackle the metric depth estimation problem from a single image. Accurate scale recovery is crucial in this context, as it directly uses depth estimation results to recover the scale of the translation vector. Despite its simplicity, the proposed method achieved the best results on the map-free validation set compared to all methods mentioned in [2]. More importantly, compared to the methods submitted to the Map-free Visual Relocalization challenge, our model has demonstrated comparable performance on the challenging test set. These metrics highlight the effectiveness of our method in addressing the challenges associated with map-free visual localization.

To sum up, our contributions are as follows:

- We propose a hierarchical matching method that integrates instance-level and feature-level approaches. This method effectively combines the strengths of global instance-level instance matching with local feature-point matching, thereby enhancing relocalization accuracy in map-free environments.
- We conducted extensive experiments on complex scenarios within the Map-free dataset, which included spatiotemporal differences, variations between different cameras, and significant parallax. These experiments demonstrate that our method exhibits superior generalization performance, surpassing existing state-of-the-art algorithms.

2 Related work

2.1 Visual Relocalization

Visual relocalization, which involves estimating camera poses from visual inputs, has been a research topic for several decades [4, 18, 22, 28, 43]. Early map-based approaches [1, 34, 44] primarily relied on image retrieval strategies to directly estimate camera poses from the most similar images in a database. From a technical perspective, these methods are mainly divided into end-to-end and modular-based approaches. For the end-to-end method [5, 15, 16, 19, 26, 36, 48, 52, 57–59], the network is trained and outputs the results directly. Some methods [6, 40, 60] calculate the absolute camera pose. For example, Chen [7] uses a scene geometry prediction module to generate the scene coordinate map, and then a Transformer-based pose regression network is used to directly retract the camera pose. Some methods [9, 17, 29, 31] calculate the relative pose. Most of them

combine camera pose regression with an information retrieval (IR) scheme [1,54]. Zhu et al. [32] investigated a hierarchical localization method that first conducts global retrieval to obtain location hypotheses, and then performs local feature matching within these candidate locations, enabling relative pose regression in large-scale environments. Turkoglu [46] combines a graph neural network and relative pose supervision to improve relocation accuracy through image retrieval and relative pose regression.

The alternative approach is based on the modular relocalization method, with key modules including feature point matching, depth estimation, and pose estimation. Some works are dedicated to feature point matching in the 2D plane. For example, LoFTR [41], which relies on the global attention mechanism of Transformers, eliminates the need for feature detectors and achieves high-precision matching through a coarse-to-fine matching strategy. SIFT [24] uses scale-invariant key points and feature vectors to achieve robust feature matching by classical feature detection and description methods. SuperGlue [33] achieves good feature detection and matching through self-supervised learning.

However, the map-based methods can only be used when there is a prior map or all the frames of the scene, and the time cost of retrieving and matching similar frames is high because it has to traverse all known frames. In recent years, map-free visual relocalization has been proposed [2,31,45], offering a more streamlined and efficient alternative to image retrieval strategies. Specifically, they utilize only two images for visual localization and do not require extensive data for pre-mapping. Some module-based methods are composed of basic methods [30,33,41] that achieve promising performance in map-free relocalization. However, any inaccuracies or errors in these modules tend to propagate to subsequent steps in the pipeline, leading to cumulative errors that ultimately degrade the overall localization accuracy.

2.2 Semantic Relocalization

Recent advancements in visual localization have significantly benefited from integrating semantic information, enhancing both accuracy and robustness. Multiple studies have employed deep learning, semantic segmentation, and geometric information to achieve these improvements.

Dynamic-SLAM [53] uses deep learning for semantic monocular visual localization and mapping, demonstrating improved performance in dynamically changing scenarios. Visual Localization Using Sparse Semantic 3D Map [37] maintains high localization accuracy under varying seasonal and lighting conditions, while Coarse-To-Fine [23] Visual Localization employs a coarse-to-fine approach using semantic compact maps for urban vehicle localization. SFD2 [55] and Visual Localization Using Semantic Segmentation and Depth Prediction [10] enhance localization accuracy through semantic-guided feature detection and the evaluation of semantic consistency during image retrieval. These methods leverage semantic information to improve the precision of visual localization. Monocular Localization with Semantics Map for Autonomous Vehicles [49] and

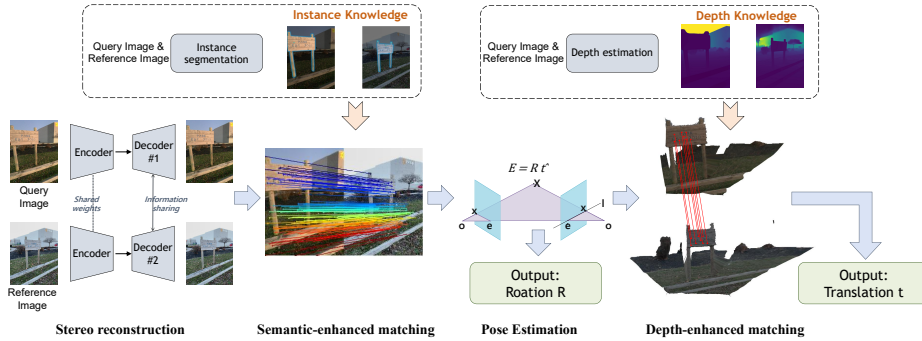


Fig. 2: Overview. Our model first takes two input images as input and obtains aligned point maps. Then, utilizing instance segmentation knowledge, feature points are matched both globally and within identified masks. The matched points are then input into an essential matrix solver, which computes the rotation matrix R and a scale-free translation vector \bar{t} . Subsequently, depth knowledge is applied to project the feature points into 3D space, allowing for the recovery of a scaled translation vector t .

Accurate Visual Localization with Semantic Masking and Attention [21] demonstrate the effectiveness of using semantic maps and attention mechanisms to enhance monocular visual localization for autonomous vehicles. Similarly, other approaches like Semantic Visual Localization [35] and Semantic Map-Based Visual Localization focus on integrating semantic information with traditional visual localization methods to improve performance in various environments. Long-term visual localization is addressed by employing semantically segmented images, ensuring robust cross-seasonal localization, as demonstrated in Long-term Visual Localization Using Semantically Segmented Images [39]. Efficient Large-Scale Semantic Visual Localization in 2D Maps [47] proposes methods for large-scale semantic visual localization within 2D maps, emphasizing efficient semantic feature matching. Other notable works include GV-Bench [56], which benchmarks local feature matching for geometric verification, Multicam-SLAM [20], which focuses on non-overlapping multi-camera SLAM for indirect visual localization, and Semantic Map-Based Localization, which integrates semantic and geometric information for improved localization accuracy.

3 Method

3.1 Overview

The overall framework of our method is shown in Figure 2. Given two input images, I_1 and I_2 , our method first utilizes feature point matching to establish a set of correspondences, which illustrate the relationship between 2D images. To enhance matching accuracy, we incorporate instance segmentation knowledge to extract the main subjects from images. Specifically, our feature point matching

algorithm is employed within the confines of this mask. Next, we use the essential matrix to compute the rotation matrix R and the scale-free unit translation vector \bar{t} from the matched 2D feature points. Finally, the depth estimation network Metric3D [14] is used to estimate the depth information of the input image which is then utilized to project the 2D matching points into the 3D space, facilitating the recovery of the final translation t .

3.2 Analysis of Intra-instance Matching

DUST3R [50] leverages 3D prior knowledge to enhance feature point matching by processing two input images, I_1 and I_2 , and outputting corresponding point and confidence maps that represent each pixel’s 3D position. The network consists of two branches, each with an image encoder, decoder, and regression head. Initially, a shared-weight Vision Transformer (ViT) encoder extracts latent representations from the input images, generating F_1 and F_2 . The decoders then use a cross-attention mechanism to facilitate information exchange between the views, refining these representations iteratively. Finally, the regression heads predict the point and confidence maps from the decoder outputs. The regression loss is based on the Euclidean distance between predicted and ground-truth 3D points, normalized by their average distances to the origin to handle scale ambiguity. This architecture effectively uses 3D prior knowledge to improve feature point matching and 3D reconstruction accuracy.



Fig. 3: The matched points within the reference and query frames show a significantly higher density within instances compared to outside instances.

We input the reference and query images into DUST3R and utilize its reconstruction mechanism to obtain only the point maps. We then match the feature points within these two point maps. Through extensive experiments, we observed that the confidence of matched points is higher within the main instance objects of the scene. As shown in Figure 3, we visualized the matched points between the

reference and query frames. Points closer to yellow indicate higher confidence, while those closer to purple indicate lower confidence. Feature point matching is more effective within the main instance objects in the scene, with almost no matched points in the background. This is due to significant parallax, illumination, and temporal changes in the background, which pose challenges for the feature point matching model during feature extraction. To address this, we introduce a feature point matching method based on semantic object knowledge, restricting the matching scope to within instances. This approach effectively avoids errors that may occur when matching points across different objects.

3.3 Instance-enhanced Matching

For a pair of images I_1, I_2 and corresponding point maps $X_{1,1}, X_{2,1}$, we aim to find the matching point. Our matching mechanism adopted the nearest neighbor matching and reciprocal matching from DUS_t3R [50]. Firstly, we use the nearest neighbor search in the 3D point map space. For each pixel (i, j) in image I_1 , we first find the corresponding 3D point $X_{1,1}(i, j)$ in $X_{1,1}$. Then we perform a nearest neighbor search in $X_{2,1}$ to localize the 3D point $X_{2,1}(k, l)$ that is closest to $X_{1,1}(i, j)$, where (k, l) are the coordinates of the matching point found in $X_{2,1}$. Then, we use reciprocal matching to improve the accuracy of the matching. From each pixel (i, j) in I_1 , we find the matching point (k, l) in I_2 . Simultaneously, from each pixel (k, l) in I_2 , we find the matching point (i, j) in I_1 . A match is considered valid only if the results are consistent in both directions, i.e., $(i, j) \leftrightarrow (k, l)$ and $(k, l) \leftrightarrow (i, j)$. We denote the global mapping as $Map^g = [((i_1, j_1), (k_1, l_1)), ((i_2, j_2), (k_2, l_2)), \dots, ((i_n, j_n), (k_n, l_n))]$, where each tuple in the map represents the matching relation between points in I_1 and I_2 , we define the $\mathcal{M}()$ as the feature point matching method:

$$Map^g = \mathcal{M}(I_1, I_2, X_{1,1}, X_{2,1}), \quad (1)$$

where the Map^g is the correspondences in global area. To significantly enhance the precision of feature point matching, instance segmentation technology was integrated, enabling the accurate extraction of primary objects from images and focusing on matching within identical instance objects. Specifically, we use SegGPT [51] to output the mask results of $Mask_1^o$ and $Mask_2^o$ for the same object in both the reference and query images. Here, $Mask_1^o$ represents the mask of the o -th in the reference frame, while $Mask_2^o$ corresponds to the mask of the same instance in the query frame. Upon obtaining the results from instance segmentation, our feature point matching algorithm conducts refined matching within these masks. Specifically, for the o -th object, we denote corresponding image as I_1^o and I_2^o , where $I_1^o = I_1 \odot Mask_1^o$, $I_2^o = I_2 \odot Mask_2^o$. Then, we perform point map reconstruction within the object and obtain corresponding point maps $X_{1,1}^o$ and $X_{2,1}^o$. Finally, we conduct matching within the mask object area:

$$Map^o = \mathcal{M}(I_1^o, I_2^o, X_{1,1}^o, X_{2,1}^o), \quad (2)$$

where the Map^o is the correspondences in the same object. This modification aims for more precise matching within individual instances, ensuring that the

feature-matching process is restricted to relevant areas defined by the instance masks. The resulting matching relationship is as follows:

$$Map(i) = \begin{cases} Map^o & \text{if } Map(i) \in Mask^o, \\ Map^g & \text{else} \end{cases} \quad (3)$$

Specifically, for areas not covered in the map, we use Map^g . For areas in the masks, we use Map^o . Overall, the utilization of instance segmentation acts as a powerful contextual aid, enhancing the understanding of the context.

3.4 Pose Estimation

For the pose solver, we selected the 5-point algorithm [27] combined with the essential matrix method as mentioned in the [2] to robustly compute the essential matrix E from matched point pairs:

$$E = U\Sigma V^T, \quad (4)$$

where U and V are orthogonal matrices representing rotation or reflection, and Σ is a diagonal matrix representing the original matrix’s stretching factor.

This matrix E is then decomposed into the rotation matrix and the scale-free translation vector. Subsequent to this decomposition, additional geometric constraints are utilized to select the correct R and \bar{t} :

$$E = \bar{t} \times R, \quad (5)$$

where \bar{t} is the scale-free translation vector, and R is the rotation matrix. Specifically, we use single-image depth estimation to back-project 2D matched points into 3D points and then evaluate which pair of R and \bar{t} ensures that the majority of these 3D points have positive depth, indicating a feasible and physically consistent configuration.

3.5 Depth-enhanced Scale Recovery

We start by transforming the input image I into a canonical camera space image I_c using camera model parameters such as focal length f^c and principal point (u^c, v^c) . The intrinsic parameters of I , including focal length f and principal point (u, v) , scale the image by the ratio $\omega_r = \frac{f^c}{f}$:

$$I_c = T(I, \omega_r), \quad (6)$$

where $T(\cdot)$ represents the image scaling operation.

Once in the canonical camera space, I_c is processed through an encoder-decoder network which initially yields a depth prediction d_c :

$$d_c = \text{Decoder}(\text{Encoder}(I_c)). \quad (7)$$

This initial depth prediction and the input image I_c are then input into a joint optimization module, which uses depth-normal consistency constraints and pseudo-normal labels for weakly supervised learning to iteratively refine depth d_c and normals N . With each iteration, the depth prediction is updated to improve accuracy and reliability:

$$d_c^{(t+1)} = d_c^{(t)} + \Delta d_c, \quad (8)$$

where $d_c^{(t)}$ is the depth prediction at the t -th iteration. Δd_c is the incremental update for the depth, representing the adjustment made in this iteration. In this way, the model incrementally adjusts the depth prediction based on new information in each iteration, continually improving the accuracy and reliability of the depth prediction. Finally, the predicted canonical depth d_c is converted back to the actual depth D in the original camera space by scaling d_c using the ratio $\omega_d = \frac{f}{f_c}$:

$$d = \omega_d d_c. \quad (9)$$

This transformation is essential to ensure the consistency of depth predictions across varying camera models, effectively accommodating different imaging conditions and maintaining the fidelity of the depth measurements. Finally, we obtain the depth of I_1 and I_2 and denote them as d_1 and d_2 , respectively.

To integrate depth information into matching, we combine the depth estimation results d_1, d_2 with matching point pairs Map from the instance-enhanced matching process. Assuming that the coordinates of a feature point pair in the reference image are (i_1, j_1) , and those of the corresponding feature point pair in the query image are (k_1, l_1) , with corresponding depth values d_1 and d_2 , we can calculate their respective 3D points using:

$$\mathbf{p}_1 = d_1 \cdot K^{-1} \begin{bmatrix} i_1 \\ j_1 \\ 1 \end{bmatrix} \quad \mathbf{p}_2 = d_2 \cdot K^{-1} \begin{bmatrix} k_1 \\ l_1 \\ 1 \end{bmatrix}, \quad (10)$$

where K represents the camera parameter matrix. \mathbf{p}_1 and \mathbf{p}_2 represents their corresponding 3D points. For each pair of 3D-3D correspondences, we compute a scale factor s of the translation vector as follows in [2]:

$$s = \frac{\|\mathbf{P}_1 - \mathbf{R}\mathbf{P}_2\|}{\|\bar{\mathbf{t}}\|}, \quad (11)$$

where $\|\mathbf{P}_1 - \mathbf{R}\mathbf{P}_2\|$ denotes the distance difference between 3D points in two images, and $\|\bar{\mathbf{t}}\|$ is the length of the translation vector. We calculate a scale factor for each pair of 3D-3D correspondences and use the RANSAC algorithm [11] to select the one with the highest agreement as the final scale factor. Finally, we transform the scale-free translation vector $\bar{\mathbf{t}}$ to the scaled translation vector $\mathbf{t} = s \times \bar{\mathbf{t}}$, combining it with the rotation matrix R to form the final relative pose of the query image with respect to the reference image.

Our comprehensive algorithm, which includes Point Map Reconstruction, Instance-enhanced Matching, Pose Estimation, and Depth-enhanced Scale Recovery, is detailed in Algorithm 1. This integrated approach ensures a robust

framework for accurate and efficient processing, leveraging each component to enhance the overall performance and precision of the system.

Algorithm 1: INFERENCE

```

1 Input: Two input images,  $I_1$  and  $I_2$ .
2 Output: Rotation matrix  $R$  and translation vector  $t$ .


---


// Point Map Reconstruction
3 calculate  $X_{1,1}$  and  $X_{2,1}$  based on Dust3R;
// Instance-enhanced Matching
4  $Mask_1, Mask_2 \leftarrow SegGPT(I_1, I_2)$ ;
5  $Map^g = \mathcal{M}(I_1, I_2, X_{1,1}, X_{2,1})$ ;
6  $Map^o = \mathcal{M}(I_1^o, I_2^o, X_{1,1}^o, X_{2,1}^o)$  based on Eq. 2;
// Pose Estimation
7  $R, \bar{t} \leftarrow E$  (Compute the rotation matrix  $R$  and the scale-free unit vector  $\bar{t}$ );
// Depth-enhanced Matching
8 calculate depth  $d_1, d_2$  of  $I_1, I_2$  based on Eq. 6,7,8,9;
9  $(x_1, y_1, z_1), \dots, (x_n, y_n, z_n) \leftarrow \mathcal{P}([(x_1, y_1), d_1], \dots, [(x_n, y_n), d_n])$  (Project the
matching points into 3D space.  $\mathcal{P}(\cdot)$  based on Eq. 10);
10  $t \leftarrow \mathcal{T}([(x_1, y_1, z_1), (x_2, y_2, z_2), \dots, (x_n, y_n, z_n)], \bar{t})$  (Recovery scale.  $\mathcal{T}(\cdot)$  based on
Eq. 11);
11 Return  $R, t$ .


---



```

4 Experiment

4.1 Dataset and Metrics

We conducted an evaluation of our method using the MapFree-Reloc dataset [2], which consists of 36,998 frames for validation and 14,778 frames for testing. The images in this dataset are from 65 validation scenes and 130 test scenes, spanning a diverse array of locations. The dataset presents difficult scenarios such as dynamic environmental conditions, dramatic viewpoint shifts, significant variability across locations, and minimal to no visual overlap with the reference image. Moreover, it is required to relocate within scenes represented by a singular reference image in map-free settings, making it more challenging. Following Map-free Relocalization [2], we use the following metrics to evaluate the performance: the Average Pose Error (the Average Median Rotation Error, the Average Median Translation Error), $AUC@VCRE < 90px$, and so on.

4.2 Performance Comparison

We analyze current models for insights into better relocalization algorithms. Specifically, we build the comparison method using three components: feature

matching methods (SIFT [25], LoFTR [42], and SuperGlue [33]), depth estimation (DPT [30] fine-tuned on KITTI [13] and NYUv2 [38]), and pose estimation (5-point solver [27] with MAGSAC++ [3], PNP [12], and Procrustes [8]). Additionally, we compared various end-to-end methods, including RPR[3D-3D]. By combining these components and end-to-end methods, we obtain 13 comparison methods. Since we don't have the ground truth of the test set, we implemented these methods on the validation set. The results are presented in Table 1.

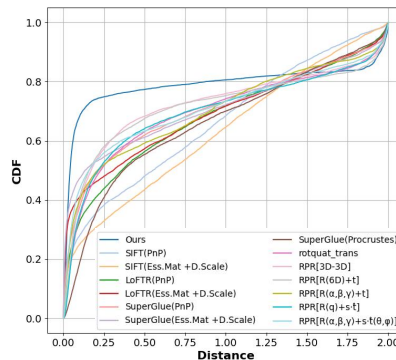
Firstly, as shown in the table with methods such as LoFTR(PnP), SIFT(PnP), SuperGlue(PnP), LoFTR(Ess.Mat +D.Scale), SIFT(Ess.Mat +D.Scale), and SuperGlue(Ess.Mat +D.Scale), different feature point matching methods (LoFTR, SIFT, SuperGlue) and pose solvers (Pnp, Ess.Mat +D.Scale) result in variations in both translation and rotation errors. This indicates that the results of feature point matching and the kind of pose solver simultaneously affect the computation of both rotation and translation. Specifically, after obtaining the coordinates of matched feature points, we use different pose solvers (such as the Perspective-n-Point (PnP), Essential matrix + depth scale (Ess.Mat. + D.Scale), or Procrustes pose solvers (Procrustes)) to compute the pose. Experimental evidence suggests that good matching, such as Ess.Mat. + D.Scale, results contribute to more accurate calculations of both the rotation matrix and the translation vector and the methods based on the essential matrix exhibit superior robustness.

For the depth estimation module, we project 2D feature points into 3D space using depth estimation results. This enables us to estimate the distances between feature points in 3D space, restoring the scale of the translation vectors obtained in the previous step and yielding the final translation vectors. Variations in depth estimation methods led to significant changes in translation errors. This comprehensive study of the interplay between feature matching, depth estimation, and pose estimation in map-free models provides valuable insights into optimizing each module to enhance overall localization accuracy.

Table 1: Quantitative comparisons on validation sets.

Method	Average Median Pose Error (m, °) @VCRE < 90px (↑)	AUC
RPR [3D-3D]	1.667m, 22.623°	0.346
RPR [R(6D)+t]	1.845m, 24.172°	0.333
RPR [R(α, β, γ) + \hat{t}]	2.543m, 33.977°	0.261
RPR [R(α, β, γ) + s · $\hat{t}(\theta, \phi)$]	1.764m, 25.349°	0.336
RPR [R(q) + t]	2.370m, 32.390°	0.290
RPR [R(q) + s · \hat{t}]	2.125m, 31.772°	0.284
LoFTR (Ess.Mat + D.Scale)	2.578m, 43.522°	0.581
LoFTR (PnP)	2.665m, 49.212°	0.569
SuperGlue (Ess.Mat +D.Scale)	2.188m, 36.358°	0.563
SuperGlue (PnP)	2.379m, 42.269°	0.541
SuperGlue (Procrustes)	2.882m, 55.455°	0.388
SIFT (Ess.Mat +D.Scale)	3.331m, 74.448°	0.395
SIFT (PnP)	3.722m, 72.291°	0.396
Ours	0.596m, 9.030°	0.591

Fig. 4: The CDF poses estimation errors across all scenes.



4.3 Main Results

Quantitative Evaluation As shown in Table 1, we first compared our method with existing approaches, and our method shows a significant reduction in Average Median Pose Error compared to the current state-of-the-art. For instance, the RPR[3D-3D] method, which performs best among the existing methods, has an Average Median Rotation Error of 22.623° , whereas ours is 9.030° . This improvement is attributed to our superior feature points matching technique. Specifically, we retain global matching information while using instance knowledge to focus the model on matching within instances. This strategy not only mitigates the impact of significant matching errors but also allows for more precise local matching. Moreover, the RPR[3D-3D] method has an Average Median Translation Error of 1.667m, while our method achieves 0.596m. This improvement is due to both our effective feature point matching and our precise depth estimation. Specifically, our method involves accurate prediction and processing of the original image depth, which is crucial for recovering the translation matrix from the scale-free translation vector. This not only confirms the effectiveness of our depth estimation approach but also highlights the importance of precise depth estimation for accurate scale recovery. Additionally, our method significantly outperforms all baseline methods in terms of the Average Median Reprojection Error, a combined measure of rotation and translation accuracy, further demonstrating the robustness and effectiveness of our approach.

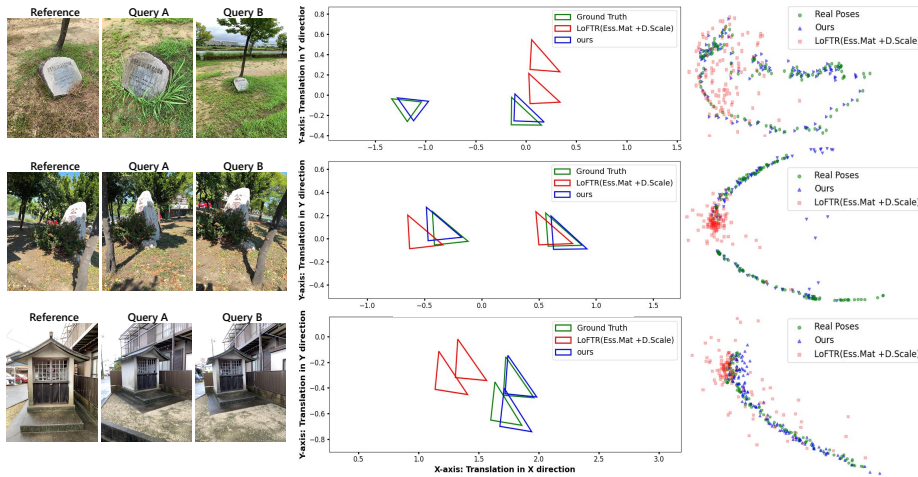
We evaluated our method’s efficacy relative to the baseline by computing the Cumulative Distribution Function (CDF) for pose estimation errors across all scenes (Figure 4). The CDF quantifies the cumulative probability of error values by sorting them in ascending order and determining the proportion below each threshold. A well-performing CDF rapidly ascends towards 1 at lower error magnitudes, indicating a predominance of lower errors. The comparative CDF curves show that our method outperforms the baseline, with our curve ascending more swiftly at reduced error levels. This demonstrates our method’s consistent lower pose estimation errors and its robustness and accuracy across various scenarios.

We also compare our method with closed-source models submitted to the Mapfree Visual Relocalization Challenge, as shown in Table 2. Our method outperforms most others, demonstrating its superiority, particularly in Median Reprojection, Median Translation, and Median Rotation Error. Additionally, the performance of our method is close to state-of-the-art methods like MAST3R (Ess.Mat + D.Scale), highlighting the significant potential of our approach.

Qualitative Evaluation We visualized the camera poses for certain frames in specific scenes on Mapfree valid sets, represented by triangles, as shown in Figure 5. In this visualization, the horizontal axis represents the displacement in the x-axis direction, while the vertical axis corresponds to the displacement in the y-axis direction. The green triangles denote the ground truth values, the blue triangles represent the camera poses estimated by our method, and the red triangles are the estimates from the baseline method, LoFTR(Ess.Mat +D.Scale). Our method’s estimates are closer to the true values, illustrating a more accurate

Table 2: Comparison on Mapfree Test sets.

Method	AUC (VCREAUC < 45px) (↑)	(VCREPrecision < 90px) (↑)	(VCREPrecision < 45px) (↑)	(VCREPrecision < 90px) (↑)	(VCREMedian Reproj .Error(px) (↓))	AUC (Err < 25cm, 5°) (↑)	Precision (Err < 25cm, 5°) (↑)	Median Trans. Error (m) (↓)	Median Rot. Error (°) (↓)
MASt3R (Ess.Mat + D.Scale)	0.817	0.933	63.0%	79.3%	48.8	0.740	54.7%	0.37	2.2
RoMa w/ MicKey depth maps	0.604	0.734	37.8%	52.4%	111.9	0.546	31.4%	1.18	15.6
DPT-KITTI & LightGlue w/ DISK	0.355	0.527	19.5%	33.2%	138.8	0.314	15.9%	1.44	18.5
SuperGlue w/ MicKey depth maps	0.556	0.711	29.8%	43.0%	139.9	0.490	23.5%	1.70	26.1
DPT-KITTI & ASpanFormer	0.414	0.641	20.8%	37.0%	161.8	0.361	16.3%	1.90	29.2
DPT-KITTI & DeDoDe (v1)	0.325	0.531	16.9%	31.2%	167.4	0.265	12.5%	2.02	30.3
Mickey Variant GT_Depth	0.548	0.720	28.0%	45.5%	142.0	0.273	10.8%	1.84	30.8
LoFTR w/ MicKey depth maps	0.550	0.715	27.2%	40.7%	155.0	0.467	20.3%	1.92	33.6
DPT-KITTI & SILK	0.192	0.312	9.8%	18.1%	176.4	0.157	7.3%	2.21	33.8
DPT-KITTI & DISK	0.346	0.536	15.1%	26.9%	208.2	0.264	10.2%	2.59	52.0
Dust3r	0.008	0.060	0.8%	6.0%	275.1	0.001	0.1%	3.01	59.2
Ours	0.656	0.849	45.3%	65.0%	80.0	0.469	28.6%	0.83	11.7

**Fig. 5:** Given a reference frame and two query frames, our model calculates the query frame pose compared to the baseline method on Ground Truth.

and reliable performance in camera pose estimation compared to the baseline. We also visualized the camera trajectories for the same scenes. Specifically, we displayed the submission results generated by our method, a baseline method LoFTR(Ess.Mat +D.Scale), and the ground truth values within the same 3D space, where each point represents a frame from the submission results. In these visualizations, green circles represent the ground truth, blue triangles denote our method, and red squares illustrate the LoFTR(Ess.Mat +D.Scale) method. As depicted in Figure 5, the LoFTR(Ess.Mat +D.Scale) method frequently exhibits anomalous outliers and even fails outright in certain scenarios. Our method consistently outperforms the baseline across multiple scenes, demonstrating both precision and robustness under various conditions.

4.4 Ablation Study

In this section, we conducted extensive ablation studies to investigate the significance of instance and depth knowledge within our framework. By isolating

Table 3: Ablation study results on Mapfree validation set, where instance knowledge and depth knowledge are ablated respectively. The case without both uses the original Dust3R pose estimation method, while using both represents our proposed method.

Instance Knowledge	Depth Knowledge	Median Trans. Error (m)	Median Rot. Error (°)	Median Reproj. Error (px)
✓		0.918	9.030	116.146
	✓	2.343	43.522	155.883
		3.291	60.093	266.326
✓	✓	0.596	9.030	70.439

and varying each component, we demonstrate on the Mapfree validation sets how the matching algorithm and depth estimation techniques affect the accuracy and robustness of the final outputs.

Instance Knowledge We ablate our instance-knowledge-enhanced feature point matching method keeping all other components unchanged (w/o instance Knowledge). Compared to our approach, it lacks instance-enhanced knowledge and superior matching techniques. As shown in Table 3, both rotation and translation errors increased. The absence of accurate feature point matches introduces significant errors when calculating the essential matrix, resulting in inaccurate rotation and translation vectors. This inaccuracy affects the final translation matrix during scale recovery. Figure 6 illustrates the increased rotation and translation errors across multiple scenarios after removing the instance knowledge.

Depth Knowledge To analyze the importance of depth knowledge, we first utilized the DPT-KITTI depth estimation method (w/o Depth Knowledge) for comparison. Additionally, we tested using the point maps directly generated by DUST3R (w/o Both) to calculate the relative poses. The results of this ablation experiment, presented in Table 3, illustrate a significant increase in the Average Median Translation Error when our depth estimation method is removed. This increase is because scale recovery relies on accurate depth estimation, where precise scale restoration directly affects the translation error metrics. Figure 6 further confirms that omitting our depth estimation method leads to increased translation errors across most scenes, indicated by larger values on the x-axis.

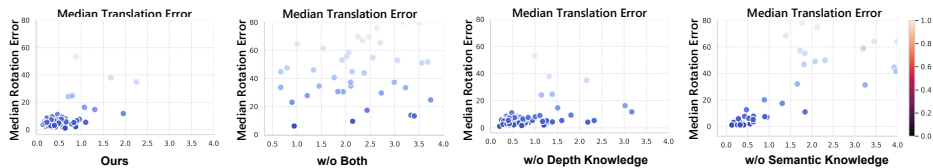


Fig. 6: Median Rotation and Translation Errors for Each scene in Mapfree validation set in the Ablation Study.

5 Conclusion

We propose a novel map-free relocalization method that estimates the relative pose of a query frame using reference and query images. By guiding the feature point matching model to focus on matches within instance objects via instance segmentation results, our approach significantly reduces incorrect matches and enhances accuracy. Additionally, we optimize 3D space point coordinates through a depth estimation for better scale recovery. Extensive experiments demonstrate the effectiveness of our collaborative optimization, paving the way for future improvements in map-free relocalization accuracy.

References

1. Arandjelovic, R., Gronat, P., Torii, A., Pajdla, T., Sivic, J.: Netvlad: Cnn architecture for weakly supervised place recognition. In: CVPR (2016)
2. Arnold, E., Wynn, J., Vicente, S., Garcia-Hernando, G., Monszpart, A., Prisacariu, V., Turmukhambetov, D., Brachmann, E.: Map-free visual relocalization: Metric pose relative to a single image. In: ECCV (2022)
3. Barath, D., Nuskova, J., Ivashechkin, M., Matas, J.: Magsac++, a fast, reliable and accurate robust estimator. In: CVPR (2020)
4. Brachmann, E., Rother, C.: Visual camera re-localization from rgb and rgb-d images using dsac. IEEE TPAMI (2021)
5. Brahmabhatt, S., Gu, J., Kim, K., Hays, J., Kautz, J.: Geometry-aware learning of maps for camera localization. In: CVPR (2018)
6. Bukschat, Y., Vetter, M.: Efficientpose: An efficient, accurate and scalable end-to-end 6d multi object pose estimation approach. arXiv preprint arXiv:2011.04307 (2020)
7. Chen, S., Cavallari, T., Prisacariu, V.A., Brachmann, E.: Map-relative pose regression for visual re-localization. In: CVPR (2024)
8. Eggert, D.W., Lorusso, A., Fisher, R.B.: Estimating 3-d rigid body transformations: a comparison of four major algorithms. MVA (1997)
9. En, S., Lechervy, A., Jurie, F.: Rpnnet: An end-to-end network for relative camera pose estimation. In: ECCVW (2018)
10. Fan, H., Zhou, Y., Li, A., Gao, S., Li, J., Guo, Y.: Visual localization using semantic segmentation and depth prediction. arXiv preprint arXiv:2005.11922 (2020)
11. Fischler, M.A., Bolles, R.C.: Random sample consensus: a paradigm for model fitting with applications to image analysis and automated cartography. Communications of the ACM (1981)
12. Gao, X.S., Hou, X.R., Tang, J., Cheng, H.F.: Complete solution classification for the perspective-three-point problem. IEEE TPAMI (2003)
13. Geiger, A., Lenz, P., Urtasun, R.: Are we ready for autonomous driving? the kitti vision benchmark suite. In: CVPR (2012)
14. Hu, M., Yin, W., Zhang, C., Cai, Z., Long, X., Chen, H., Wang, K., Yu, G., Shen, C., Shen, S.: Metric3d v2: A versatile monocular geometric foundation model for zero-shot metric depth and surface normal estimation. arXiv preprint arXiv:2404.15506 (2024)
15. Kendall, A., Cipolla, R.: Modelling uncertainty in deep learning for camera relocalization. In: ICRA (2016)

16. Kendall, A., Cipolla, R.: Geometric loss functions for camera pose regression with deep learning. In: CVPR (2017)
17. Khatib, F., Margalit, Y., Galun, M., Basri, R.: Grelpose: Generalizable end-to-end relative camera pose regression. arXiv preprint arXiv:2211.14950 (2022)
18. Kim, M., Koo, J., Kim, G.: Ep2p-loc: End-to-end 3d point to 2d pixel localization for large-scale visual localization. In: ICCV (2023)
19. Laskar, Z., Melekhov, I., Kalia, S., Kannala, J.: Camera relocalization by computing pairwise relative poses using convolutional neural network. In: ICCVW (2017)
20. Li, S., Pang, L., Hu, X.: Multicam-slam: Non-overlapping multi-camera slam for indirect visual localization and navigation. arXiv preprint arXiv:2406.06374 (2024)
21. Li, T., Zhan, Z., Tan, G.: Accurate visual localization with semantic masking and attention. EURASIP Journal on Advances in Signal Processing (2022)
22. Li, Y., Snavely, N., Huttenlocher, D., Fua, P.: Worldwide pose estimation using 3d point clouds. In: ECCV (2012)
23. Liao, Z., Shi, J., Qi, X., Zhang, X., Wang, W., He, Y., Liu, X., Wei, R.: Coarse-to-fine visual localization using semantic compact map. In: 2020 3rd International Conference on Control and Robots (ICCR). IEEE (2020)
24. Lowe, D.G.: Distinctive image features from scale-invariant keypoints. IJCV (2004)
25. Lowe, D.G.: Distinctive image features from scale-invariant keypoints. IJCV (2004)
26. Melekhov, I., Ylioinas, J., Kannala, J., Rahtu, E.: Image-based localization using hourglass networks. In: ICCVW (2017)
27. Nistér, D.: An efficient solution to the five-point relative pose problem. IEEE TPAMI (2004)
28. Panek, V., Kukulova, Z., Sattler, T.: Visual localization using imperfect 3d models from the internet. In: CVPR (2023)
29. Rajendran, P.K., Mishra, S., Vecchietti, L.F., Har, D.: Relmobnet: End-to-end relative camera pose estimation using a robust two-stage training. In: ECCV (2022)
30. Ranftl, R., Bochkovskiy, A., Koltun, V.: Vision transformers for dense prediction. In: ICCV (2021)
31. Rockwell, C., Kulkarni, N., Jin, L., Park, J.J., Johnson, J., Fouhey, D.F.: Far: Flexible accurate and robust 6dof relative camera pose estimation. In: CVPR (2024)
32. Sarlin, P.E., Cadena, C., Siegwart, R., Dymczyk, M.: From coarse to fine: Robust hierarchical localization at large scale. In: CVPR (2019)
33. Sarlin, P.E., DeTone, D., Malisiewicz, T., Rabinovich, A.: Superglue: Learning feature matching with graph neural networks. In: CVPR (2020)
34. Schindler, G., Brown, M., Szeliski, R.: City-scale location recognition. In: CVPR (2007)
35. Schönberger, J.L., Pollefeys, M., Geiger, A., Sattler, T.: Semantic visual localization. In: Proceedings of the IEEE conference on computer vision and pattern recognition (2018)
36. Shavit, Y., Ferens, R., Keller, Y.: Learning multi-scene absolute pose regression with transformers. In: ICCV (2021)
37. Shi, T., Shen, S., Gao, X., Zhu, L.: Visual localization using sparse semantic 3d map. In: 2019 IEEE international conference on image processing (ICIP). IEEE (2019)
38. Silberman, N., Hoiem, D., Kohli, P., Fergus, R.: Indoor segmentation and support inference from rgb-d images. In: ECCV (2012)
39. Stenborg, E., Toft, C., Hammarstrand, L.: Long-term visual localization using semantically segmented images. In: 2018 IEEE international conference on robotics and automation (ICRA). IEEE (2018)

40. Stoffl, L., Vidal, M., Mathis, A.: End-to-end trainable multi-instance pose estimation with transformers. arXiv preprint arXiv:2103.12115 (2021)
41. Sun, J., Shen, Z., Wang, Y., Bao, H., Zhou, X.: Loftr: Detector-free local feature matching with transformers. In: CVPR (2021)
42. Sun, J., Shen, Z., Wang, Y., Bao, H., Zhou, X.: LoFTR: Detector-free local feature matching with transformers. In: CVPR (2021)
43. Svärm, L., Enqvist, O., Kahl, F., Oskarsson, M.: City-scale localization for cameras with known vertical direction. IEEE TPAMI (2016)
44. Torii, A., Arandjelovic, R., Sivic, J., Okutomi, M., Pajdla, T.: 24/7 place recognition by view synthesis. In: CVPR (2015)
45. Tu, D., Cui, H., Zheng, X., Shen, S.: Panopose: Self-supervised relative pose estimation for panoramic images. In: CVPR (2024)
46. Turkoglu, M.O., Brachmann, E., Schindler, K., Brostow, G.J., Monszpart, A.: Visual camera re-localization using graph neural networks and relative pose supervision. In: 3DV (2021)
47. Vojir, T., Budvytis, I., Cipolla, R.: Efficient large-scale semantic visual localization in 2d maps. In: Proceedings of the Asian Conference on Computer Vision (2020)
48. Walch, F., Hazirbas, C., Leal-Taixe, L., Sattler, T., Hilsenbeck, S., Cremers, D.: Image-based localization using lstms for structured feature correlation. In: ICCV (2017)
49. Wan, J., Zhang, X., Dong, S., Zhang, Y., Yang, Y., Wu, R., Jiang, Y., Li, J., Lin, J., Yang, M.: Monocular localization with semantics map for autonomous vehicles. arXiv preprint arXiv:2406.03835 (2024)
50. Wang, S., Leroy, V., Cabon, Y., Chidlovskii, B., Revaud, J.: Dust3r: Geometric 3d vision made easy. In: CVPR (2024)
51. Wang, X., Zhang, X., Cao, Y., Wang, W., Shen, C., Huang, T.: Seggpt: Segmenting everything in context. arXiv preprint arXiv:2304.03284 (2023)
52. Xian, K., Shen, C., Cao, Z., Lu, H., Xiao, Y., Li, R., Luo, Z.: Monocular relative depth perception with web stereo data supervision. In: CVPR (2018)
53. Xiao, L., Wang, J., Qiu, X., Rong, Z., Zou, X.: Dynamic-slam: Semantic monocular visual localization and mapping based on deep learning in dynamic environment. Robotics and Autonomous Systems (2019)
54. Xu, Y., Shamsolmoali, P., Granger, E., Nicodeme, C., Gardes, L., Yang, J.: Transvlad: Multi-scale attention-based global descriptors for visual geolocalization. In: WACV (2023)
55. Xue, F., Budvytis, I., Cipolla, R.: Sfd2: Semantic-guided feature detection and description. In: Proceedings of the IEEE/CVF Conference on Computer Vision and Pattern Recognition (2023)
56. Yu, J., Ye, H., Jiao, J., Tan, P., Zhang, H.: Gv-bench: Benchmarking local feature matching for geometric verification of long-term loop closure detection. arXiv preprint arXiv:2407.11736 (2024)
57. Zhang, J., Yang, G., Tulsiani, S., Ramanan, D.: Ners: Neural reflectance surfaces for sparse-view 3d reconstruction in the wild. NeurIPS (2021)
58. Zhang, J.Y., Pepose, S., Joo, H., Ramanan, D., Malik, J., Kanazawa, A.: Perceiving 3d human-object spatial arrangements from a single image in the wild. In: ECCV (2020)
59. Zhang, J.Y., Ramanan, D., Tulsiani, S.: Relpose: Predicting probabilistic relative rotation for single objects in the wild. In: ECCV (2022)
60. Zhen, J., Fang, Q., Sun, J., Liu, W., Jiang, W., Bao, H., Zhou, X.: Smap: Single-shot multi-person absolute 3d pose estimation. In: ECCV (2020)